Long-Term Stability of an Area-Reversible Atom-Interferometer Sagnac Gyroscope

D. S. Durfee
Department of Physics and Astronomy, Brigham Young University, Provo, Utah 84602, USA

Y. K. Shaham
Department of Physics, Yale University, New Haven, Connecticut 06520-8120, USA

M. A. Kasevich
Department of Physics, Stanford University, Stanford, California 94305-4060, USA
(Received 27 October 2005; published 15 December 2006)

We report the first demonstration of a matter-wave interference gyroscope that meets both the short-term noise and long-term stability requirements for high accuracy navigation. This performance level resulted from implementation of a novel technique to precisely reverse the input axis of the gyroscope.

DOI: 10.1103/PhysRevLett.97.240801 PACS numbers: 06.30.Gv, 03.75.Dg, 32.80.Lg, 39.20.+q

In recent years the noise performance of laboratory de Broglie wave gyroscopes [1] has rivaled that of the best rotation sensors, including, for example, large area ring laser gyroscopes [2] and low-noise mechanical gyroscopes [3]. However, the utility of de Broglie wave sensors for applications in basic science and technology hinges not only on their short-term noise performance but also on their long-term stability. For example, high accuracy terrestrial navigation requires a stable rotation output at the ~ 1 mdeg/h level for time scales ~ 84 min [4,5]. Geodetic applications, such as detection of wobble in the Earth rotation rate, require stability at the level of ~ 1 μdeg/h over months [6].

In this Letter, we report the demonstration of the first atom interferometric gyroscope which meets the stringent stability requirements for high accuracy navigation [4,5]. In particular, by observing the gyroscope rotation output in a nearly static environment, we demonstrate a gyroscope bias stability of <70 μdeg/h, scale factor stability of <5 ppm, and short-term noise of ~ 3 μdeg/h$^{1/2}$ [7]. Taken together, these parameters enable navigation at a level where system drift is significantly less than 1 km/h [5]. We obtain this performance through implementation of a precise electro-optic reversal of the gyroscope input axis.

We employ sequences of light pulses to coherently manipulate atomic wave packets [8]. The presence of a perturbing inertial force changes the relative phase between the atomic de Broglie waves and the optical fields and, as described below, allows for precise characterization of the inertial force. This method is well suited to high accuracy navigation applications because distances are referenced to the wavelength of frequency stabilized lasers and atoms propagate in a nearly force-free environment along space-time geodesics.

In our work, these pulses excite two-photon stimulated Raman transitions between the $F = 3$, $m_F = 0$ and $F = 4$, $m_F = 0$ ground state hyperfine levels of atomic Cs in a $\pi/2 - \pi - \pi/2$ excitation sequence [9]. The first $\pi/2$ pulse places the atoms into an equal superposition of $F = 3$ and $F = 4$ states and gives the $F = 4$ component two-photon recoils of momentum when the Raman transitions are driven in the counterpropagating beam configuration (atoms are initially prepared in the $F = 3$ state). After a time delay T, the π pulse exchanges the internal electronic states and external momentum states associated with the two atomic wave packets. This causes their paths to converge after another time interval T. The final $\pi/2$ pulse results in the interference of the overlapping wave packets. The fraction of atoms in the $F = 4$ state, from which the rotation rate of the apparatus is determined, is probed by resonance fluorescence.

The output transition probability P can be written as $P = \frac{1}{2}[1 - \cos(\phi_a + \phi_s)]$, where ϕ_a is determined by the relative motion of the atomic wave packets with respect to the laser fields and contains the desired inertial phase shift, as described below, while ϕ_s parametrizes spurious noninertial phase shifts (such as those induced by stray magnetic fields) which do not depend on the orientation of the Raman laser propagation vectors. To an excellent approximation [10], $\phi_a = \mathbf{k}_1 \cdot (\mathbf{x}_1^a - \mathbf{x}_1^0) - 2\mathbf{k}_2 \cdot (\mathbf{x}_2^a - \mathbf{x}_2^0) + \mathbf{k}_3 \cdot (\mathbf{x}_3^a - \mathbf{x}_3^0)$. Here the subscript indexes each of the three successive Raman interactions, $\mathbf{x}_i^a$ is the semiclassical position of the atom at the time of the interaction (neglecting laser momentum recoil) in a nonrotating, inertial coordinate system, $\mathbf{x}_i^0$ is the phase reference for the optical fields, and $\mathbf{k}_i = \mathbf{k}_i^{(1)} - \mathbf{k}_i^{(2)}$ is the effective Raman propagation vector ($\mathbf{k}_i^{(1)} \simeq -\mathbf{k}_i^{(2)}$ are the propagation vectors associated with each of the two frequency components used to drive the Raman transitions). Assuming the atoms have initial velocity $\mathbf{v}_0$ and the effective Raman propagation vectors initially have common orientations $\mathbf{k}_0$ which rotate with angular rate $\mathbf{\Omega}$, it is straightforward to show that

$$\phi_a = \mathbf{k}_0 \cdot [(2\mathbf{v}_0 \times \mathbf{\Omega})T^2 + \mathbf{x}_0]. \quad (1)$$

We previously demonstrated that the $\mathbf{x}_0$ term can be separated from the desired rotation term by using a counterpropagating atomic beam geometry in which interferometer outputs are simultaneously acquired for atomic beam velocities $\mathbf{v}_0$ and $-\mathbf{v}_0$, because the rotation dependent term reverses sign with velocity, while the $\mathbf{x}_0$ term does not.

In our apparatus a pair of horizontally oriented, counterpropagating, Cs atomic beams (longitudinal velocity of $\sim$220 m/s) propagate down the length of a $\sim$2 m long ultrahigh vacuum chamber [1,11]. They intersect three pairs of horizontally oriented, counterpropagating laser beams whose propagation axes are orthogonal to the atomic beams. Before interacting with the laser fields, the atoms are collimated using transverse laser cooling and optically pumped into the $F = 3$ ground state. This combination of parameters results in a phase shift of 9.1 rad for a rotation rate equal to Earth's rotation rate ($\Omega_E =$ 15 deg/h). Typical interference fringes for the co- and counterpropagating atomic beams are shown in Fig. 1(a). Fringes were acquired using an electro-optic technique to bias the interferometer at Earth rotation rate and to scan the interference fringes [1]. This was accomplished by applying small additional frequency offsets to the Raman difference frequencies for the $\pi/2$, π and final $\pi/2$ pulses, respectively.

We located the interferometer directly on the floor of our laboratory, with minimal vibration isolation. This was done to reduce errors due to slow drifts in the orientation of the apparatus resulting from the use of compliant shock mounts. Our laboratory was located in the basement of the building with the slab of the laboratory floor in direct contact with the Earth below. The high frequency noise observed on the traces in Fig. 1(a) is due to rotation noise in the laboratory building associated with air handlers, pumps, and nearby roads. We characterized this noise by acquiring rotation signals in an unmodulated operation mode where each rotation output was tuned to the side of the interference fringe. While this mode is ideal for characterizing high frequency noise sources, it is unsuitable for long records as it does not control for drifts in interference fringe contrast or atom flux. The rotation noise spectrum is shown in Fig. 1(b). The root power spectral density of the angular motion (angle random walk) reaches a nearly atom shot-noise limited baseline of 3×10^{-6} deg/h$^{1/2}$ from 2 to 7 Hz. This noise level is roughly 1000 times better than that associated with ring laser gyroscopes or fiber optic gyroscopes in navigation grade inertial navigation systems [12]. The substantially higher noise at frequencies outside of this band reflects the rotation noise in our laboratory, and sets the limit for the acquisition noise for the long-term drift data reported below.

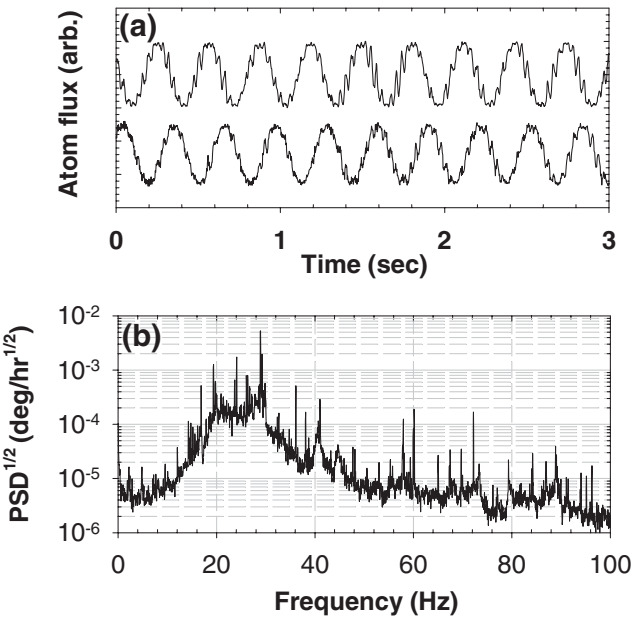

FIG. 1. (a) Typical interference fringes. Upper trace: copropagating atomic beam. Lower trace: counterpropagating atomic beam. (b) The square root of the spectral density of the cultural rotation noise in the laboratory.

To suppress the spurious phase shift term ϕ_s, we implemented a k-vector (case) reversal in which the direction of the propagation vector $\mathbf{k}_0$ was periodically reversed (e.g., $\mathbf{k}_0 \rightarrow -\mathbf{k}_0$). This had the effect of reversing the sign of inertial phase shifts while leaving the sign of the ϕ_s unchanged. The corrected (case-compensated) rotation output was obtained by subtracting phase shifts obtained from the standard rotation output ($\mathbf{k}_0$) from the case-reversed rotation output ($-\mathbf{k}_0$). Because each rotation output itself is obtained by subtracting phase shifts from co- and counterpropagating atomic beams, implementation of this method required acquisition of four interference signals.

We implemented the case reversal through electro-optic frequency shifts of the laser beams used to drive the Raman transitions. The essential feature of this implementation is that it achieved an effective reversal of the Raman momentum transfer while otherwise precisely maintaining the spatial alignment of the laser beam propagation axes. Many other envisioned methods (such as those employed, for example, in Ref. [13]) couple minor laser beam misalignments to the reversal mechanism, and thereby introduce systematic spurious drifts in the rotation output.

The details of the reversal method are as follows. The Raman resonance is driven when the difference frequency between two counterpropagating laser beams is resonant with the ground state hyperfine transition frequency (the resonance linewidth of $\sim$100 kHz was determined by the transit time of an atom through the light fields). In order to achieve the resonance condition, we first generated a pair of copropagating beams whose frequency difference was equal to ground state hyperfine frequency plus or minus a

small (5 MHz) frequency offset [14]. The offset was chosen to be sufficiently large to suppress the Raman resonance for the copropagating fields. This beam was divided three ways and steered into the apparatus to create the $\pi/2$, π and $\pi/2$ interaction regions. After passing once through the atomic beams, each laser beam pair was directed through acousto-optic frequency modulators and then retroreflected back into the apparatus. The modulators were configured to upshift the optical frequencies of the counterpropagating beam pair by the same (5 MHz) offset frequency. The Raman resonance was then obtained with one frequency from the forward propagating beams and one from the counterpropagating beams. Near perfect case reversal was achieved by switching between the plus and minus initial frequency offsets. This had the desired effect of reversing the sign of the effective Raman propagation vector [15].

Figure 2 shows data which demonstrate the efficacy of the case-reversal technique. Figure 2(a) shows the phase shifts extracted from the interference fringes for the standard (case 0) and case-reversed (case 1) outputs and the case-compensated output obtained from these traces. For this record every other data point was taken in the case-reversed configuration. The phase for each case was acquired by subtracting the phases obtained from fitting sinusoids to 66 sec interference fringe records for both the co- and counterpropagating atomic beams. The strong anticorrelation of the two cases and the much lower drift in the average phase demonstrates the utility of case reversal for increased stability.

Several of our data sets showed windows of low drift in the case-compensated output. One such 7×10^3 sec window occurred between 9×10^3 and 1.6×10^4 sec for the data shown Fig. 2(a). The Allan deviation of the data for this interval is shown in Fig. 2(b). At $\sim 2 \times 10^3$ sec it reaches a minimum value of 6.3×10^{-5} rad or

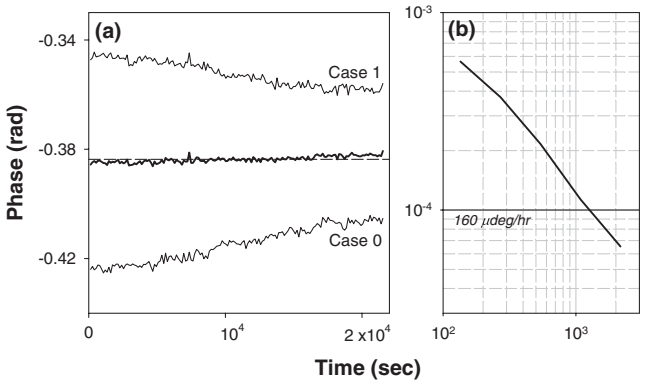

FIG. 2. (a) Measured phases over a 2×10^4 sec period. The interferometer phase of the case-reversed (case 1) trace has been multiplied by -1 such that a positive phase change indicates a positive rotation change in both traces. The dark trace indicates the case-compensated output. (b) Allan deviation for the interval between 9×10^3 and 1.6×10^4 sec.

103 μdeg/h. This minimum places an upper limit on the potential bias stability of the gyroscope. Using the methods described in Ref. [16] we estimate a bias stability of 68 μdeg/h. For comparison, compensated commercial navigation grade ring laser gyroscopes have bias stabilities of ~ 2 mdeg/h.

The performance of many gyroscopes is improved by removing known correlations of the rotation output with other measured parameters [12]. For our work we recorded 29 auxiliary environmental parameters in addition to the rotation signals. These parameters included Raman laser pointing, intensity and frequency, magnetic fields, and temperatures at many locations in the apparatus. The rotation output showed strong correlation with five of these temperatures. A simple least-mean-squares correction, in which these measurements were each multiplied by a constant and subtracted from the phase at every point in time, considerably reduced drift. In an integrated navigation systems, such correlations would be removed using, for example, an optimal Kalman filter [17]. Figure 3(a) shows a typical case-compensated output record and its correlation with a linear sum of five temperature measurements. Figure 3(b) shows the temperature-compensated output. The Allan deviation for signals corrected in this way is plotted in Fig. 3(c). The corrected signal's bias stability is 67 μdeg/h at 1.7×10^4 sec. Comparison with Fig. 2(c) indicates that further improvements may be possible with more complete error models. This data also imply a drift in the scale factor of less than five parts per million, because the gyroscope is operating under the constant Earth rate rotation bias.

Finally, we have performed extensive studies to determine the physical origin of these correlations. The dominant source of correlations are temperature driven alignment errors in the Raman optics paths and temperature driven drifts in the Raman laser intensities [18]. Figure 4 shows the sensitivity of the apparatus output to

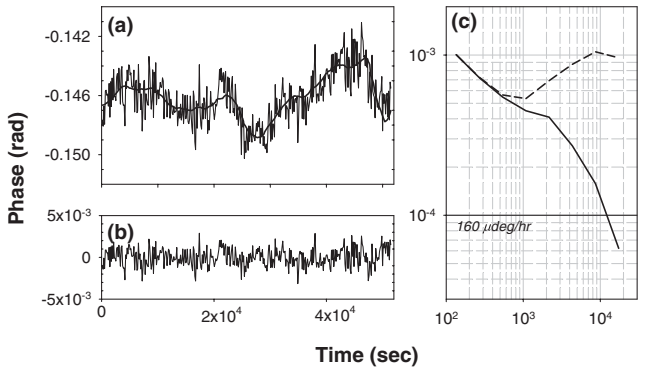

FIG. 3. (a) Case-compensated output (light line) and correlation signal (dark line) consisting of a linear sum of five temperature measurements. (b) Temperature-compensated rotation output. (c) Allan deviation for the case-compensated (dashed line) and temperature-compensated (solid line) signals.

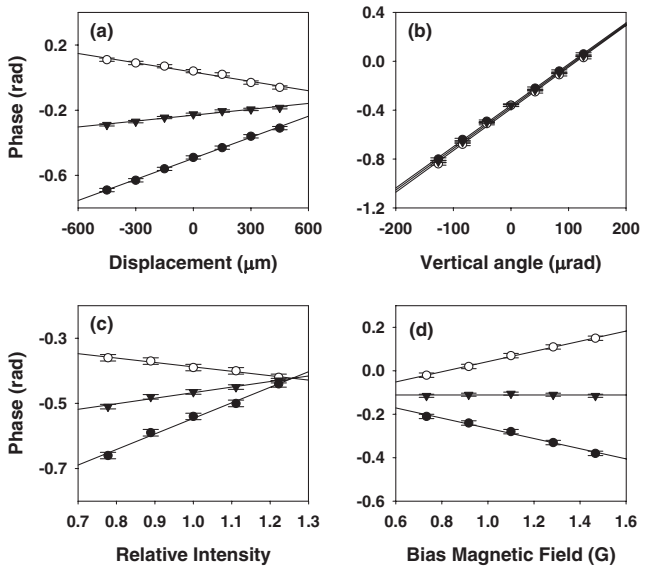

FIG. 4. The standard (solid circles), case-reversed (open circles), and case-compensated outputs (triangles) for (a) longitudinal displacement of the π pulse, (b) vertical deflection of the first $\pi = 2$ laser beam retro-reflection, (c) fractional change in Raman laser intensity, and (d) magnetic field bias current.

these perturbations for a particular apparatus alignment, for each case orientation and for the case-compensated output. Figure 4(a) shows a 0.12 mrad case-compensated output phase shift per 1 μm displacement of the position of the center π pulse along the length of the apparatus. Figure 4(b) shows a 3.3 mrad case-compensated output phase shift for a 1 μrad vertical deflection of the first $\pi/2$ laser beam retroreflection. Figure 4(c) shows a 1.7 mrad shift per 1% change in the Raman laser intensity. The Raman laser intensity was stable at the 0.5% rms level over 10^4 sec. This correlation results from a subtle dependence of the effective atomic beam velocity $\mathbf{v}_0$ on the Raman laser intensity, because the π and $\pi/2$ pulse conditions depend on the product of Raman beam intensity and the atom's time of flight through the laser fields. Figure 4(d) shows the sensitivity to longitudinal magnetic field gradients, and was obtained by changing the bias field current. The phase shift for each case resulted from a 5% magnetic bias field inhomogeneity along the length of the apparatus. The case-compensated output is insensitive to magnetic field fluctuations, because the dominant contribution to this shift is independent of the direction of $\mathbf{k}_0$. Allan variance analysis demonstrates that the correlation coefficients are stable over 20 h data runs. We find that the optimal correlation coefficients differ following a full reoptimization and realignment of the apparatus, because these coefficients depend on the relative alignments of the optical fields and the atomic beams.

In conclusion, we have demonstrated a matter-wave gyroscope which meets the demanding performance requirements for high accuracy navigation. Future work will focus on refinement of the instrument error models, and instrument engineering for nonlaboratory, navigation, environments.

We acknowledge helpful discussions with J. M. McGuirk, J. B. Fixler, G. T. Foster, and G. Nogues. This work was supported by the National Science Foundation, the Office of Naval Research, and NASA.

[1] T. L. Gustavson, A. Landragin, and M. A. Kasevich, Classical Quantum Gravity **17**, 2385 (2000).
[2] C. H. Rowe *et al.*, Appl. Opt. **38**, 2516 (1999); R. W. Dunn *et al.*, Appl. Opt. **41**, 1685 (2002).
[3] J. Gilmore *et al.*, Proc. SPIE-Int. Soc. Opt. Eng. **4632**, 38 (2002).
[4] A. Chatfield, *Fundamentals of High Accuracy Navigation* (AIAA, Reston, VA, 1997).
[5] C. Jekeli, *Inertial Navigation Systems with Geodetic Applications* (de Gruyter, New York, 2001).
[6] K. U. Schreiber *et al.*, J. Geophys. Res. **109**, B06405 (2004).
[7] Bias stability is the parameter that characterizes the stability of the sensor output under null input conditions. Scale factor is the multiplicative constant that relates the input rotation rate to the gyroscope signal output.
[8] P. Berman, *Atom Interferometry* (Academic Press, San Diego, 1997).
[9] M. Kasevich and S. Chu, Phys. Rev. Lett. **67**, 181 (1991).
[10] K. Bongs, R. Launay, and M. A. Kasevich, Appl. Phys. B **85**, 602 (2006); Ch. Antoine, and C. J. Bordé, J. Opt. B **5**, S199S207 (2003); B. Dubetsky and M. Kasevich, Phys. Rev. A **74**, 023615 (2006).
[11] T. L. Gustavson, P. Bouyer, and M. A. Kasevich, Phys. Rev. Lett. **78**, 2046 (1997).
[12] A. Lawrence, *Modern Inertial Technology* (Springer, New York, 1998).
[13] M. J. Snadden, J. M. McGuirk, P. Bouyer, K. G. Haritos, and M. A. Kasevich, Phys. Rev. Lett. **81**, 971 (1998).
[14] The two lasers were tuned 850 MHz below the $6^2S_{1/2}$ $F = 3$ and $F = 4$ to $6^2P_{3/2}$ $F = 3$ allowed optical transitions.
[15] To be explicit, $\nu_+^{(2)} = \nu_+^{(1)} + \nu_{\rm hfs} + S\Delta\nu$, $\nu_-^{(2)} = \nu_+^{(1)} + \nu_{\rm hfs} + S\Delta\nu + \Delta\nu$, and $\nu_-^{(1)} = \nu_+^{(1)} + \Delta\nu$. Here the subscript indicates propagation direction, the superscript the Raman frequency component, ν is the laser beam frequency, $\nu_{\rm hfs}$ is the hyperfine resonance, $\Delta\nu$ is the 5 MHz frequency shift, and $S = +1$ or -1 is the sign of the shift. The relevant Raman frequencies are $\nu_+^{(2)} - \nu_-^{(1)}$ and $\nu_-^{(2)} - \nu_+^{(1)}$.
[16] L. C. Ng and D. J. Pines, J. Guid. Control. Dyn. **20**, 211 (1997). The bias stability B is obtained by multiplying the minimum Allan deviation by 0.6648.
[17] M. Grewal and A. Andrews, *Kalman Filtering* (Wiley, New York, 2001).
[18] Measured laboratory temperature fluctuations were at the 0.01 °C rms level.